Available online at www.sciencedirect.com
ScienceDirect
Vibrational Spectroscopy 41 (2006) 144–154
VIBRATIONAL SPECTROSCOPY
www.elsevier.com/locate/vibspec

Towards T-ray spectroscopy of retinal isomers: A review of methods and modelling

I. Jones *, T.J. Rainsford, B. Fischer, D. Abbott

Centre of Biomedical Engineering and Department of Electrical and Electronic Engineering, The University of Adelaide, SA 5005, Australia

Received 4 November 2005; received in revised form 2 December 2005; accepted 5 December 2005
Available online 19 January 2006

Abstract

The *terahertz gap* lies between the infrared and millimeter regions of the electromagnetic spectrum. Terahertz (THz) waves, or T-rays, bridge the gap between electronics and photonics, have novel properties and interact uniquely with many materials. Various rotational, vibrational and translational modes of molecules are within the THz range (0.1–10 THz). Since these modes are unique to a particular molecule it is possible to obtain a 'THz fingerprint' allowing for the identification of chemical substances. Astronomers and chemists have already utilised the THz region to characterise and identify small organic molecules. Terahertz spectroscopy allows not only for exploration of molecular structures but also for molecular dynamics. One difficulty in performing THz spectroscopy is that the data can be noisy and thus difficult to interpret. An a priori knowledge of the expected THz spectra allows improved experiments to be performed. Ab initio molecular orbital theory is a helpful tool in providing a great deal of information about intermolecular structure, interactions and dynamics. Recently, we have begun to investigate whether THz is a useful part of the spectrum for studying the photoisomerization of the retinal chromophore by using molecular modelling and vibrational mode calculations. The vibrational character of very low frequency modes can provide insight into molecular dynamics since they potentially relate to the torsional coordinates relevant to the actual isomerization itself. To date, very few studies on the retinal molecule and its isomers based on THz technology have been carried out. Initial experiments using THz Time-Domain Spectroscopy (THz–TDS) have shown that it is possible to distinguish between the different isomeric forms of retinal, indicating that the THz modality may be useful for studying very low frequencies and associated mechanics. In order to motivate further THz experiments on retinal, this paper reviews: (i) the status of the retinal chromophore, (ii) the work in the area uptil now, and (iii) the background of THz spectroscopy—furthermore we review and perform ab initio calculations for all-*trans* and 9-*cis* retinal in the THz regime.

Keywords: T-rays; THz spectroscopy; Retinal isomers; Ab initio molecular modelling

1. Introduction

Vibrational spectroscopy has long been used to detect vibrational marker modes, which allow for the identification of unknown substances [1,2]. It also provides insight into structural dynamics, for example, intramolecular hydrogen transfer, biomolecular proton transfer, and *cis–trans* isomerization in retinal proteins [3]. Such dynamics, which are elementary steps in chemistry typically take place on femtosecond to picosecond timescales [4]. Since the development of short-pulsed laser systems, ultrafast chemistry has been studied mainly using time-resolved electronic spectroscopy. The disadvantage of probing electronic transitions is the overlapping of relatively featureless transient electronic bands of stimulated emission and contributions of excited state absorption [5]. On the other hand, structural resolving techniques such as time-resolved X-ray [6], X-ray spectroscopy [7], and electron diffraction [8] are technologically demanding. Recent developments in ultrafast laser technology have enabled the efficient generation of tunable femtosecond laser pulses from the UV through to the very far-infrared regions of the electromagnetic spectrum [9,10].

However, different spectroscopic information may be obtained from different regions of the electromagnetic spectrum. Infrared spectroscopy provides information about individual bond lengths and angles of various molecules, whereas various rotational, vibrational and translational modes of molecules are located within the far-infrared region. The terahertz (or T-ray)

* Corresponding author. Tel.: +61 883036296.
E-mail address: ijones@eleceng.adelaide.edu.au (I. Jones).

0924-2031/$ – see front matter © 2005 Elsevier B.V. All rights reserved.
doi:10.1016/j.vibspec.2005.12.005

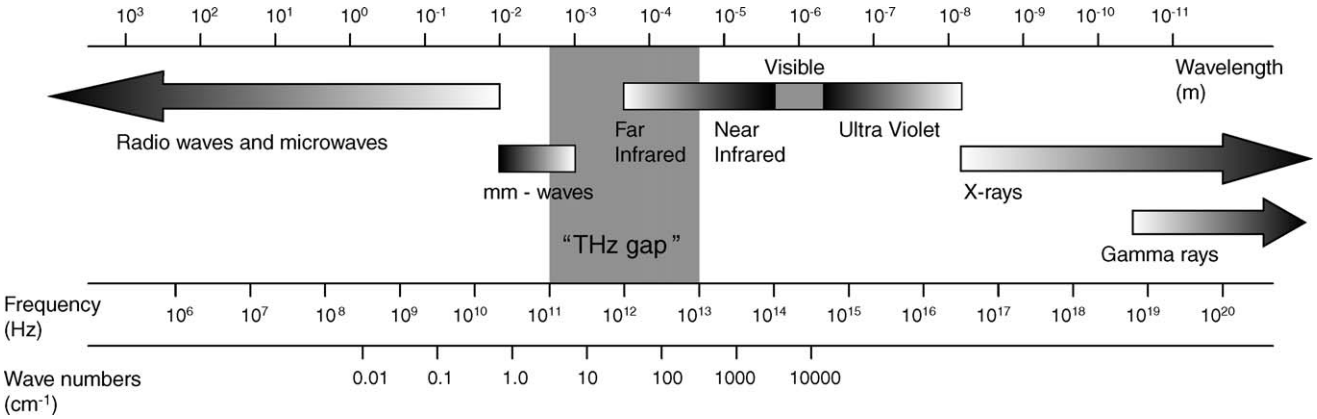

Fig. 1. The electromagnetic spectrum. A representation of the electromagnetic spectrum, showing the 'Terahertz (THz) gap' between the well-developed fields of millimeter waves (mm-waves) and the infrared. The T-ray band lies between 0.1 and 10 THz.

frequency range (0.1–10 THz or 3–333 cm^{-1} in wavenumbers), which straddles the mm-wave and very far IR bands (see Fig. 1), can provide direct information about intermolecular or phonon modes, for example those characterising a crystalline structure [11]. These modes are often unique to a particular molecule, allowing for the identification of unknown chemical substances through a spectral 'terahertz fingerprint' [12]. Terahertz techniques, complement Raman and IR spectroscopy, having similar instrumentation, sample preparation, and analysis methods.

Terahertz can provide solutions to a number of difficulties that are encountered with Raman spectroscopy techniques. For instance, due to the proximity of the visible excitation line, low frequency modes are difficult to assess in Raman. Further, because Raman spectroscopy involves high powered laser irradiation it can induce phase changes and initiate photochemical reactions. Such problems occur in the study of polymorphs and isomers where discrimination is required in, for example, finished pharmaceutical products. Being able to accurately differentiate between various isomeric and polymorphic structures is essential for a number of applications in biomedicine and pharmaceuticals as well as for security applications. For example, Taday et al. [13,14] have shown that it is possible to differentiate between the different isomers that are present in paracetamol (2-acetamidophenol, 3-acetamidophenol and 4-acetomidophenol) by comparing their THz spectra. Such applications are further supported by the fact that plastic and polyethylene packaging is transparent to THz. This allows for better environmental control of samples and also for the direct inspection of packaged materials for quality control monitoring as THz spectroscopy can be applied, for example, while tablets are in blister packets. Thus THz can be used to monitor changes that are related to time, pressure, and temperature without influencing the phase or chemically changing the pharmaceutical. Terahertz also does not generate fluorescence, which can be a problem for Raman spectroscopy [15].

In near-infrared (NIR) spectroscopy the situation becomes more complex because the measured spectra consist of many combination and overtone bands of the fundamental mid-infrared (MIR) vibrations, making analysis difficult.

Terahertz exhibits a number of further advantages. Sampling times are less than 200 ms, and are speeding up as the technology advances, which opens up possibilities for high-throughput applications such as fast DNA sensing for microarrays.

The vibrational character of very low frequency modes can provide new insight into molecular mechanics since they potentially relate to the torsional coordinates relevant to the actual isomerization. Most molecules have dense and distinctive absorption spectra at THz frequencies, which has led to much interest in THz spectroscopy [11,16–18]. Using THz transmission or reflection spectroscopy, samples ranging from gases to solids can be completely characterised at THz frequencies. The density of molecular twisting and bending modes in the THz band provides a wealth of information about the composition and state of the samples [19,20].

Pulsed THz techniques are based on ultrafast lasers, where the femtosecond regime allows for the possibility of studying molecular dynamics. The ability of THz to follow dynamical changes at the molecular level has caught the attention of many researchers. For example Upadhya et al. [21] used a time-resolved broadband (100 GHz–12 THz) THz spectroscopy system to study the far-infrared vibrational modes of crystalline saccharides, and to understand the dynamics of both inter- and intramolecular interactions. We have begun to explore the potential of THz for distinguishing between various isomeric forms of a molecule, studying conformational changes in proteins and other biomolecules. A knowledge of the protein dynamics is widely useful to researchers in areas from molecular simulation in HIV research [22], optical memory devices [23] and artificial vision [24,25] through to novel technologies such as nano-mechanical switches [26]. In particular we are exploring the various isomers of retinal. A great deal is already known about retinal's isomers and its related proteins [27,28,30,31]. Currently, very few THz studies of retinal have been carried out. The work of Walther et al. [32] has shown that it is possible to identify the different isomeric structures of retinal using THz spectroscopic data. This result indicates that it is worth carrying out further studies in order to look at these lower frequencies more comprehensively and also shows that THz is a useful regime for our ultimate aim of studying retinal dynamics.

One difficulty in performing THz spectroscopy is that the data can be noisy at the limits of the dynamic range and thus difficult to interpret. An a priori knowledge of the expected THz spectra allows improved experimentation. Molecular modelling, especially ab initio molecular orbital theory in combination with quantum mechanics and molecular mechanics (QM/MM), has recently become a useful tool in the support of spectroscopic data as well as in gaining information about intermolecular structure, interactions and dynamics [33–36]. Modelling allows for the visualization and study of the conformation and structure of a molecule, the study of mechanisms of reactions, and comparison of molecules with each other. Modelling the *cis–trans* isomerization of the retinal molecule can potentially provide information about the structure of intermediates as well as vibrational frequencies and dynamics. We use ab initio molecular orbital calculations to find frequencies in the THz range and to assign their vibrational modes.

The aim of this present work is to determine through ab initio calculations the frequencies and corresponding modes in the THz frequency range of 0.1–6 THz of the all-*trans* and *cis* isomers of retinal. In order to motivate and meet this aim the paper is structured in the following way. Section 2 provides a brief overview of the retinal chromophore and its proteins. Due to space considerations we have limited ourselves to the chromophore itself and not studies of the associated proteins, bacteriorhodopsin and rhodopsin, except in a few cases of particular interest. This is followed by Section 3, which gives an up to date overview of experimental approaches ranging from early crystallographic studies through to recent Raman studies. In limiting ourselves we have placed an emphasis on studies of the structure of the various isomers and intermediates involved in the isomerization process. Because our main interest lies in the application of THz spectroscopy this section also provides background information on THz techniques. Section 4 then gives an introduction to different molecular modelling techniques and an overview of relevant modelling approaches of retinal. After this we present our own ab initio calculations of two different retinal isomers in Section 5 and compare them with existing data from both modelling and experiment. We find these results to be compatible with the existing IR [33], ab initio [34], and THz data [32] and they motivate the need to carry out spectroscopy at these lower frequencies.

2. The retinal chromophore

Visual pigments, which are found in both vertebrates and invertebrates, are members of a protein class called "G-protein coupled receptor proteins." In vertebrates, rhodopsin, also known as visual purple, is a photoreceptor protein bound to its chromophore, i.e. retinal. In the vertebrate retina, rhodopsin is responsible for the primary events in the detection of light [37,38]. It catalyses the only light sensitive step in vision and is found, for example, in the rod cells of the vertebrate visual system [27].

Halophilic archea, such as *Halobacterium halobium* or *Halobacterium salinarum* contain four different retinal proteins; the light-driven ion pumps bacteriorhodopsin (proton pump) and halorhodopsin (chloride pump) [39,40] as well as the phototactic receptors sensory rhodopsin I and sensory rhodopsin II [41,42]. Bacteriorhodopsin is a photosynthetic pigment similar to rhodopsin and is found in the purple membrane of halophilic bacteria [43]. It has photoreactions similar to those observed in rhodopsin and functions as an energy transducer or proton pump [44,45].

All of these pigments such as rhodopsin and related bacteriorhodopsin have in common that they all comprise seven transmembrane helices and are composed of a retinylpolyene chromophore bound to a parent opsin protein [27]. Although the majority of (vertebrate) visual pigments employ a protonated Schiff base formed with a lysine residue, the UV-sensitive pigments appear to be unprotonated [28]. The retinal chromophores occur in different isomeric forms depending on the physical function of the protein. In rhodopsin (for vertebrates), 11-*cis* retinal is covalently bound to opsin and the photoisomerized all-*trans* form is eventually released, which then must be reconverted to 11-*cis* retinal. However, in certain invertebrates, such as insects however, the active form of rhodopsin, metarhodopsin, is thermally stable and is thus photoisomerized back to 11-*cis* retinal [29].

Bacteriorhodopsin, halorhodopsin and the two sensory rhodopsins contain the all-*trans* isomer of retinal that is photoisomerized to 13-*cis* is retinal [37,38]. The light-driven pumps bacteriorhodopsin and halorhodopsin use the energy stored in the 13-*cis* is form of retinal to drive ion transport across the membrane. The transition between photointermediates can be correlated with the transfer of ions within the transmembrane pore. In sensory rhodopsin I and II, the 13-*cis* form of retinal signals the activated state, which is forwarded along the signal transduction cascade by specifically associated transducer proteins. The fact that it is all-*trans* retinal in some cases and 11- or 13-*cis* in others can be explained by looking at the physical function of the different proteins. Such physiological processes differ significantly amongst the various proteins, for example, in the case of rhodopsin in the vertebrate visual system it is neuron transduction and in bacteriorhodopsin it is the cross membrane proton pump. Visual chromophores, for example, in rhodopsin, are sensitive to an extremely wide spectrum of light, where different rhodopsins display distinct absorption maxima, for example $\sim$ 500 nm for rhodopsin (in humans) and $\sim$ 568 nm for bacteriorhodopsin, which are thought to be determined by interactions between the residues in the transmembrane segments and the chromophore [46]. Also, the 11-*cis* form gives the chromophore the ability to adopt an infinite number of conformations along its conjugated polyene chain [47]. The ability for such fine tuning is unnecessary for the pigments of *H. halobium*.

The first step in the transduction process is the isomerization of retinal. In bacteriorhodopsin this initiates a series of events that includes the release of the Schiff base proton to the outside of the cell, its reprotonation from the cytoplasmic side and the ultimate return of the protein and retinal to their starting states. The resulting transmembrane proton gradient drives other cellular functions, while the whole transduction process takes around 10 ms. The changes in retinal and the protein are

reflected in spectral changes due to the formation and decay of intermediates K_{605}, L_{550}, M_{410}, N_{560}, and O_{640}[48,49]. In each of these, the retinal is in a transition state between the *cis* and the *trans* form. The combination of structural, spectroscopic and biochemical analysis have allowed for the determination of the likely path of the proton as it traverses the membrane [50–52].

Visual transduction in rhodopsin is initiated by photons, which lead to the isomerization of 11-*cis* retinal to all-*trans* retinal. This conformational change distorts the protein to a high-energy form, called bathorhodopsin [27]. Subsequently, a series of rapid thermal transitions occur, in which the protein again alters shape, and within a few milliseconds adopts a form called metarhodopsin II, which can activate the phototransduction cascade. Eventually, the high chromophore/protein distortion energy results in the thermal relaxation of the protein conformation, which finally leads to the expulsion of retinal from opsin as its all-*trans* isomer [47].

During the photocycle, changes occur to the retinal chromophore as well as to the entire protein. Changes in the retinal binding pocket cause structural modification of the retinal molecule. The *cis–trans* isomerization is the fastest known biological photochemical reaction ($\sim$ 200 fs) [53,54]. Vibrational coherence of the isomerization may be responsible for the speed of this reaction. The initial excited state dynamics along the C_{11}=C_{12} torsion may direct the correct distortion of the chromophore. Indeed, studies with chromophores, which lack intramolecular steric interactions, isomerize on a slower time scale (400–600 fs) and produce a smaller quantum yield [55]. Vibrational coherence has previously been observed in the reactant state of the photosynthetic reaction centre of bacteria prior to ultrafast electron transfer [55]. This has led to a series of experimental studies of the role of vibrational coherence in chemical and biological reactions, which since then has been observed in various biologically important molecules [56,57].

3. Experimental approaches

Having briefly reviewed the retinal chromophore, we now review various spectroscopic techniques in the context of retinal research. Section 3.1 briefly overviews X-ray techniques and Section 3.2 reviews infrared techniques, thereby placing into context the new THz methods described in Section 3.3.

Researchers have long been interested in the mechanism of the photocycle and hence the retinal molecule. Electron microscopy and X-ray crystallography have provided a great deal of information about structure and dynamics of retinal. One approach to studying the nature of structural changes is to use conditions that prolong the life of the structural intermediates, such as lower temperature, adding in additives, and the use of genetically altered variants of the protein. Spectroscopic studies have characterised vibrational modes and are useful in predicting possible structures of intermediates as well as providing information about molecular mechanics. Different information can be gained about a molecule depending on which part of the spectrum is being explored. The region that has long been of most interest for chemical analysis is the mid-infrared region (4000–400 cm^{-1}), which corresponds to changes in vibrational energies within molecules. However, information about dynamics is contained within the far-infrared part of the spectrum and beyond (400–10 cm^{-1}), especially below 200 cm^{-1}. It is rarely possible to identify an unknown compound using IR spectroscopy alone. Being able to interpret the terahertz spectrum of a molecule and assign its low frequency vibrational modes would allow for more precise identification. Terahertz spectroscopy is a potentially useful modality for explaining intermediates and dynamics. Ultrafast changes in absorption spectra can be seen with pump–probe experiments using a THz pulse duration of less than a picosecond.

3.1. Crystallography

The first structural analysis of bacteriorhodopsin was carried out using electron microscopic imaging [58]. An atomic model was determined [59] that has since been confirmed by a number of studies [60–62]. Studies using electron and X-ray crystallographic techniques have provided a plethora of models for the structure of bacteriorhodopsin: for example, see Subramian et al. [63] for an excellent review including a table of results. The X-ray data is at a typically higher resolution and the data of Luecke et al. [64] is likely to be the most accurate.

Studies on the retinal chromophore in rhodopsin include Okada et al. [65], who used a new 2.2 Å crystal structure to provide details of the chromophore binding site including the configuration about the C_6–C_7 single bond of the 11-*cis*-retinal Schiff base. They also revealed a significant negative pre-twist of the C_{11}=C_{12} double bond.

3.2. Infrared and Raman spectroscopy

Bacteriorhodopsin (bR), halorhodopsin (hR) and sensory rhodopsin (sR) I and II have similar atomic masses ($\sim$ 26,000 Da) and photocycles but their physiological roles are very different. Rhodopsin is difficult to work with since it is not photostable. Bacteriorhodopsin on the other hand can withstand a larger photon flux. This is why a great deal more is known about the chromophore and its intermediate structures for bacteriorhodopsin [66–69] and halorhodpsin [70–73] compared to rhodopsin [28,74]. Very little is known about sensory rhodopsin I [75].

To observe and analyse the ultrafast isomerization process of bacteriorhodopsin, early picosecond optical studies [76] were used, which suggested that a primary photoproduct ‘‘K’’ occurred in 11 ps. In 1978, Ippen et al. [77] measured the formation of the photoproduct within 1 ps. Later it was shown that a redshifted precursor to the intermediate K, called J, forms in approximately 500 fs and relaxes to K on a 3 ps time scale [78–80]. A further species I_{460} has been observed and assigned to the excited state intermediate to J [78]. In 1988, Mathies et al. [69] used femtosecond spectroscopy, which achieved time resolutions of 6 fs. Hence, they were able to probe the coherent vibrational motion of retinal after photoexcitation, which allowed them to observe the time course of the double-bond isomerization in bacteriorhodopsin. Doig et al. [81] used the

same method to show the existence of further intermediates that occur during the transduction of bacteriorhodopsin, i.e. J_{625}. They established that there may also be a I_{460}. There is some controversy over J_{625} and I_{460} in terms of their structure. Modelling may provide insight although one needs to consider not just the retinal molecule itself, but also the influence of the binding pocket. This has a significant affect on the ultrafast response timescale and has been described before [64].

In 1991, Schoenlein et al. [53] first reported femtosecond absorption spectra of bovine rhodopsin and concluded that the formation of the photoproduct was completed in only 200 fs. The idea of an extremely fast isomerization also matched with the results of Peteanu et al. [82]. The results were interpreted in terms of rapid deformation around the C_{11}=C_{12} double bond occurring as fast as vibrational motions of the chromophore. Coherent isomerization of rhodopsin was first reviewed in 1994 [83] and later confirmed by various studies [84,85]. It was concluded that the vibrationally coherent *cis–trans* isomerization can lead to the high reaction quantum yield of rhodopsin. The yield of the rhodopsin chromophore (a protonated Schiff base of 11-*cis* retinal) in solution ($\sim$ 0.15) [86,87] is much smaller than that in protein bound form (0.67) [88], indicating that the isomerization of the rhodopsin chromophore is much enhanced in the protein environment of rhodopsin.

Initial studies on sensory rhodopsin I using Raman spectroscopy [75] obtained vibrational spectra of the native membrane bound form of sR_{587} and used these data to determine the structure of its retinal prosthetic group. The similar frequencies and intensities of the skeletal fingerprint modes in sR_{587}, bacteriorhodopsin (bR_{568}), and halorhodopsin (hR_{578}) demonstrate that the retinal chromophore has an all-*trans* configuration bound to the protein by a protonated Schiff base linkage, which is weakly hydrogen bonded with its protein. This suggests that the red shift in the absorption maximum compared to bR and hR is likely due to a reduction in electrostatic interaction between the protonated Schiff base and its protein counterion.

Preresonance Raman difference spectra for isolated all-*trans* retinal compared to the protein bound isomer were obtained by Senak et al. [89] in 1996. They used a CCl_4 solution as a diluent, complexed with cellular retinol-binding protein (CRBPI). The spectra indicated that retinal has a slightly more planar conformation within the binding pocket of CRBPI than in solution. Vibrational modes in the fingerprint region (1000–1400 cm^{-1}), which were affected by the binding CRBPI, were observed and compared with early results from studies undertaken in 1971 [90–92]. In 1997 Lin et al. [36] carried out low-frequency Raman spectroscopy of 11-*cis* retinal in rhodopsin and bathorodopsin, the *trans* primary photoproduct that showed a relatively strong Raman response. These revealed that the photoexcited chromophore undergoes rapid nuclear motion along torsional coordinates, which may be involved in the 200 fs isomerization about the C_{11}=C_{12} bond.

3.3. Ultrafast THz spectroscopy

Ultrafast THz generation and detection uses the ultra-broadband nature of femtosecond (fs) optical laser pulses to reach the THz region of the spectrum. Pulsed T-ray radiation consists of ultrashort pulses, with a bandwidth spanning the range from approximately 0.1 to 10 THz (3–333 cm^{-1}), covering the THz Gap. The femtosecond laser pulses are fired at a photoconductor or a crystal, and thereby generate THz electromagnetic transients that can be detected [93]. Through a beam splitter and a synchroniser, the laser pulses are forced to strike the THz generator and detector with a known phase coherence. A time-dependent waveform proportional to the THz field amplitude and containing the frequency response of the sample can then be produced by scanning the time delay and sampling the signals on the detector (Fig. 2).

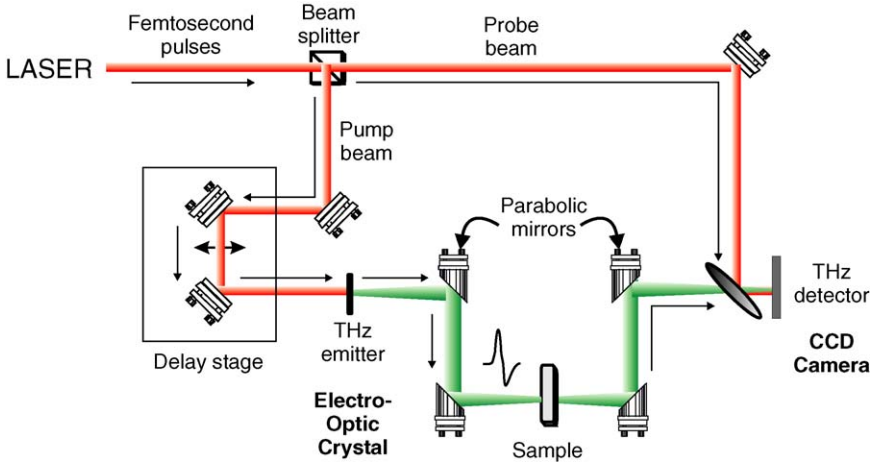

Fig. 2. Illustration of a transmission THz–TDS system. The ultrafast laser beam is split into pump and probe beams. The pump beam is incident on the THz emitter to generate THz pulses and the THz pulses are collimated and focused on the target using parabolic mirrors. After transmission through the target the THz pulse is collimated and refocused on the THz detector. The optical probe beam is used to gate the detector and measure the instantaneous THz electric field. A delay stage is used to offset the pump and probe beams and allow the THz temporal profile to be iteratively sampled. However, note that the CCD camera is only necessary for fast imaging, and use of a single photodetector is an alternative. Whilst this example shows a THz system in transmission mode, it should be noted that reflective mode measurements are also well established. Figure adapted from Nature Materials [94].

The two main applications in which THz techniques are involved are THz spectroscopy and THz imaging. THz Time-Domain Spectroscopy (THz–TDS) and related THz technologies, especially THz wave (T-ray) imaging modalities provide spectroscopic information, such as functional imaging [95] and has the potential to impact on an almost limitless number of interdisciplinary fields including communications [96], imaging [97–99], medical diagnosis [100], health monitoring [101], environmental control [102], and chemical [20] and biological identification [94,103,104]. T-rays do not subject biological tissue to harmful ionizing radiation, because they maintain low-photon energy (∼4 meV at 1 THz) [105], in comparison to typical X-ray photon energy that is in the order of keV. In addition to imaging, THz systems can also provide spectroscopic information such as unique rotational, vibrational and translational responses of materials and therefore enable molecular fingerprinting with T-rays [95].The potential of THz spectroscopy has been realized for a variety of applications. A number of researchers have measured the THz spectra of various substances of interest in security and defence [106], medical research [107], and molecular science [108,109].

Walther et al. [32] have used THz time domain spectroscopy to measure the FIR spectra of three isomers of retinal: all-*trans*, 13-*cis* and 9-*cis*. Their observations show that there are distinct differences between the low frequency vibrational spectra of the three isomers. Also by comparing the three isomers they were able to deduce the approximate localization of the different vibrational modes within a molecule. However, they only measured the spectra between 0.3 and 3 THz and therefore only observed a small number of vibrational modes. A broader view of the THz spectrum of these isomers, for example between 0.1 and 6 THz, would give better insight into the molecular dynamics and would further enable localization of the modes within the molecules.

4. Ab initio molecular modelling

Having reviewed various experimental spectroscopic techniques, we have motivated the context for THz spectroscopy. Our aim is now to briefly overview the molecular modelling techniques that will be applied to retinal in Section 5 along with a brief overview of past molecular modelling approaches applied to retinal.

Modelling techniques allow any chemical species to be studied in detail. For example, in our case, calculations can be performed on the reactive intermediates that are difficult to investigate experimentally. Information can be gained about the reactive transition structures and excited states—sometimes it is only possible to obtain this information by calculation. Complete sets of data can be obtained and calculations can be carried out on structures artificially constrained to allow individual interactions to be assessed. There is a wide range of molecular modelling and quantum chemistry software available and different researchers have made use of different techniques depending on their research goals.

The ab initio approach to chemistry is that the Schrödinger equation leads to the direct quantitative prediction of chemical phenomena using only Planck's constant, the speed of light and the masses and charges of electrons and nuclei. Of course very few problems are tractable and so approximate mathematical models of the Schrödinger equation for which the solutions may exist are used. There are two distinctly different approaches to approximating solutions of Schrödinger's equation. The first is to solve the problem at the highest level of theory. This is only possible for very small systems such as the hydrogen molecule. The second approach is to solve a theoretical model for which a number of characteristics must hold true: the model should be unique, well defined, continuous, unbiased, and relative errors should increase in proportion to the size of the molecule. It should also yield a total energy that is an upper bound to that which would result from an exact solution of the full Schrödinger equation. Such a model should also be implementable on a computer with minimal computational effort. The most commonly used models of this class are those which are based on molecular orbital theory: the approximate treatment of electron distribution and motions, which uses one-electron functions or orbitals to approximate the full wave equation. A many-electron wavefunction is constructed from the molecular orbitals in the form of a determinant. Such models have been validated through systematic comparison with experimental data. Individual molecular orbitals are expressed as linear combinations of a finite set of one-electron functions known as basis functions. The choice of basis set determines the level of accuracy and depends on two components: (a) the size of the basis set and (b) the treatment of electron correlation. In general the choice of basis set will always be a compromise.

Typical engines used for ab initio calculations are Gamess [110] and Gaussian [111,112]. Here, ab initio calculations themselves can be divided into quantum mechanics and molecular mechanics/dynamics. In general, quantum methods are slow but potentially very accurate, and require huge memory and CPU resources, which limit their application to relatively small molecules. On the other hand they provide full simulations of all the properties and fine behaviour of the molecules. For bigger molecules, methods with a reasonable accuracy requiring less computation time are needed. Molecular mechanics and molecular dynamics (MM/MD) methods treat atoms as spheres with charge, and bonds as springs. They do not consider independent subatomic particles, and as such are more limited in their utility.

Such calculations begin with specifying the bond lengths and angles. Often information about symmetry can greatly reduce the time required for integral evaluation. Programs such as Gaussian and Gamess have incorporated many standard basis sets although non-standard sets can be specified in detail for each atom if required. First, integrals are calculated and a guess at the wavefunction made. Execution proceeds into a programmed loop where the self-consistent field (SCF) equations are solved for the total energy and wavefunction. First derivatives of the energy with respect to the displacements in the nuclear coordinates are evaluated. If the wavefunction (gradient of the energy) is below some preset limit then the originally specified geometry represents within some limit a

stationary point on the potential energy surface. The optimization procedure then terminates. Otherwise the original geometry is varied and a new calculation of integrals, SCF and energy gradient follows.

Once the correct molecular geometry is obtained, other calculations such as the vibrational frequencies, IR and Raman spectra, excitation energies and related properties of excited states may be calculated. A number of other more advanced quantum mechanical methods have been used recently [33,36,114]. Examples include multiconfiguration self-consistent field theories, density functional theory and the consistent force-field method. We have chosen to use ab initio techniques, in the first instance, which are well documented, easy to use and widely available.

4.1. Modelling of retinal

In 1997, Gervasio et al. [33] published the first report on ab initio calculations on low frequency modes of a retinal isomer. The infrared and Raman spectra of all-*trans*-retinal were obtained at room temperature and at 15 K. Aside from these experiments, ab initio calculations of vibrational frequencies based on density functional theory were carried out. Frequencies between 17 and 334 cm^{-1} were recorded. Frequencies and normal modes were also calculated using the density functional approach B3-LYP. This showed that many of the vibrational modes are located on the ring or chain fragment of molecule and that the chain torsational modes are of primary interest for the photoisomerization process.

Lin et al. [36] used QCFF/PI (Quantum Mechanical Extension of the Consistent Force-Field Method) for the calculation of mode frequencies of rhodopsin, isorhodopsin, bathorhodopsin and two different protonated Schiff bases. The consistent force-field method belongs to the group of methods called molecular mechanics where the potential energy of a molecule, a molecular complex or a crystal is calculated as a sum of inter-atomic potentials, whose parameters are ideally obtained by optimization on experimental structural and spectroscopic data for the pure substances. Subsequent to these calculations the resulting frequencies were compared with relative Raman intensities and excited-state displacements and the good agreement of those enabled approximate location of the vibrational modes. However, no frequencies under 90 cm^{-1} were calculated or measured.

More recently, Morari and Bogdan [35] used ab initio and vibrational self-consistent field (VSCF) computations to investigate the vibrational normal coordinates of the protonated Schiff base (PSB) of 11-*cis* retinal. These studies focused on the normal coordinates modes that involve the central C= C bond, which plays a significant role in the isomerization process. The calculations were performed at the Restricted Hartree-Fock (RHF) level with Pople's N-31G split valence basis set. Light atom polarization functions were also used (RHF/6-31G*). Anharmonicity correction were taken into account by using the correlation-corrected vibrational SCF (VSCF) method. Vibrational frequencies of 270, 328 and 998 cm^{-1} were reported with relatively large corrections. It was found that those vibrational bands contribute significantly to the rotation around the angles most important in promoting the isomerization process.

Quantum mechanics and molecular mechanics methods (QM/MM) can also be used to analyse the influence of the protein environment on the photoisomerization process. Roehrig et al. [115] suggested with the help of hybrid QM/MM simulations that the photoreaction in rhodopsin is limited to a single pathway, which is essentially determined by steric constraints. It was also confirmed that the protein binding pocket selects and accelerates the isomerization exclusively around the C_{11}=C_{12} bond via preformation of a twisted structure, that this all-*trans* isomerization produces a highly strained chromophore, and that the photon energy in bathorhodopsin is stored in internal strain of the reprotonated Schiff base (RPSB) and in steric interaction energy within the protein. The conclusion of these studies was that the initial step of vision can be viewed as the compression of a molecular spring and that the highly specific alteration of the protein environment is a result of its strain release.

In 2005, Blomgren and Larsson [114] investigated the influence of two different QM/MM methods on the calculated frequencies. The reason for this was that variants of the Hartree-Fock SCF procedure are all single determinant solutions. Other approaches include the MCSCF multiconfiguration SCF. This procedure consists of using many (more than one) Slater determinants. One implementation is the CASSCF, the complete active space SCF. Blomgren and Larsson [114] investigated the ground state of the retinal molecule and while doing so compared the results of two different QM/MM methods. It was found that density functional theory (DFT) and complete active space multiconfiguration SCF (CASSCF) produce different results for bond length alternation in a model system of retinal. It is also stated that the two methods deal with the steric constraint imposed by the protein by producing different values of the twist angles in the carbon chain. These differences in results were found to be related to the positively charged nitrogen of the Schiff base, which leads to different p-bond orders produced by the two methods. For an uncharged model the two methods were proven to agree rather well. Basis sets 6-31G (without polarization functions) and 6-31G* (with light atom polarization functions) were used in these calculations.

5. THz modelling of retinal

In this section we now apply the techniques reviewed in Section 4 in order to obtain predicted vibrational frequencies of all-*trans* and 9-*cis* retinal in the THz region.

The calculations of the structure and vibrational frequencies of all-*trans* and 9-*cis* retinal were carried out with ab initio methods using the GAMESS-UK electronic structure package [110] and the visualization programs Molden [113] and GaussView [111,112]. The calculations included optimization of the molecular structures initially using the minimal basis set STO-3G (Slater-Type Orbital), later Pople's split valence basis set 6-31G** with light and heavy atom polarization functions. A low gradient convergence tolerance was used, which was increased with each optimization step. The frequency calcula-

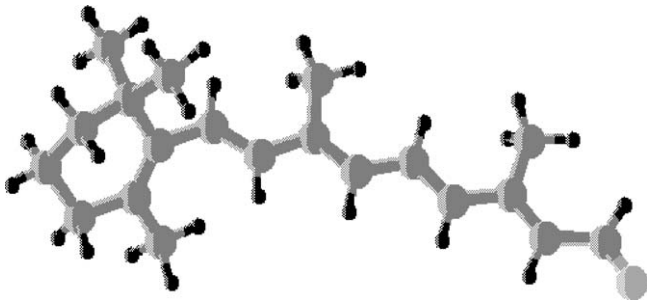

Fig. 3. The all-*trans* retinal isomer visualized in Molden [113], optimized with Gamess [110].

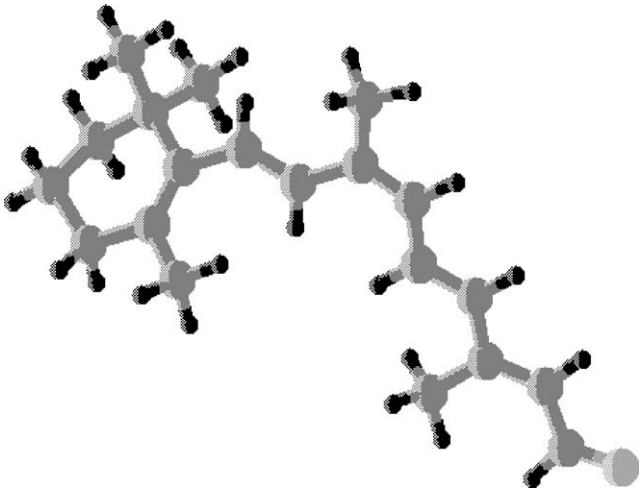

Fig. 4. The 9-*cis* retinal isomer visualized in Molden [113], optimized with Gamess [110].

tions were carried out by calculating the Hessian using the same basis set and tolerance as in the last optimization. The modelled and optimised structures of all-*trans* and 9-*cis* retinal are shown in Figs. 3 and 4.

The calculated vibrational spectra of all-*trans* and 9-*cis* retinal in the range from 0.1 to 6 THz (3–200 cm^{-1}) are shown

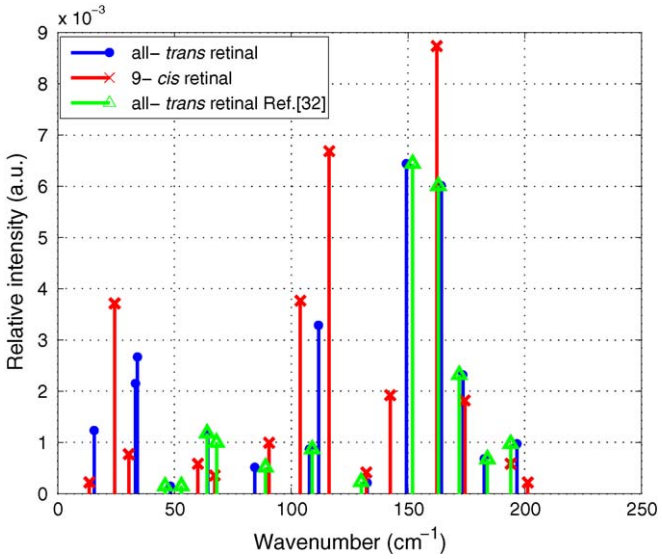

Fig. 5. The calculated THz spectra of all-*trans* and 9-*cis* retinal in comparison to each other and to experimental data [33]. The spectra cover the region of approximately 0.1–6 THz ($\sim$ 3–200 cm^{-1}). The intensities are shown in arbitrary units, where the highest intensity of the full spectrum of each molecule was equated with 1.0 and all other frequencies were normalised to this value. The reference experimental data is included only in consideration of the frequency modes, not their absolute intensities as only relative values were provided by the previous study.

in Fig. 5. An assignment of the locations of the vibrational modes and a further comparison with two references [32,33] is shown in Tables 1 and 2. It should be noted that the description of the vibrational modes is simplified and based on the normal mode representation in Molden [113]. In Table 2, we have not assigned our calculated band at 60.09 $cm^{-1}$to Walter et al.'s experimental value of 53.9 cm^{-1}: Walter et al. modelled their experimental data in the spectral region 40–75 cm^{-1}using a standard expression for the Lorentzian oscillators. In order to reproduce the progression of their experimental data curves they needed to add three extra modes into the model centered at 62.1, 65.9 and 74.5 cm^{-1}. Their additional mode at 62.1 cm^{-1}

Table 1
Calculated low frequency vibrational modes (wavenumbers in cm^{-1}) of all-*trans* retinal compared to experimental results

Ref. [33]	Ref. [32]	This work	Assignment
–	–	15.59	Ring, chain torsion
–	–	33.27	Ring, chain, bending in plane
–	–	34.16	Ring, chain out of plane
46	47	48.31	Chain torsion, first double bond
53	54	–	–
–	61	–	–
64	66	64.39	Ring bending
68	69	–	–
89	90	84.42	Chain bending
109	–	107.75	Ring, chain bending, in plane
–	–	111.74	Ring methyl group torsion, chain methyl group bending
130	–	132.46	Ring methyl group torsion
152	–	149.31	Ring methyl group torsion, chain H–C═ O bending
163	–	164.31	Ring, chain (both) methyl group torsion, H– C═ O bending
172	–	173.55	Chain (terminal) methyl group torsion
184	–	182.60	Ring, chain (middle) methyl group torsion
194	–	196.61	Ring, chain (both) methyl group torsion

Table 2
Calculated low frequency vibrational modes (wavenumbers in cm^{-1}) of 9-*cis* retinal compared to experimental results

Ref. [32]	This work	Assignment
–	13.62	Ring, chain torsion
–	24.40	Ring, chain bending, out of plane
43.5	30.41	Ring, chain bending in plane
53.9	–	–
–	60.09	Ring bending
–	67.22	Ring, chain bending
–	90.58	Chain (both) methyl groups bending
–	103.93	Ring, chain bending, in plane
–	116.27	Ring methyl group torsion, chain (both) methyl group bending
–	132.29	Ring methyl group torsion
–	142.44	Ring methyl group torsion
–	162.33	Ring, chain (terminal) methyl group torsion, H–C═ O bending
–	174.36	Chain (terminal) methyl group and terminal chain torsion
–	193.97	Ring, chain (terminal) methyl groups torsion

is much closer to our calculated mode at 60.09 cm^{-1} than there experimental mode at 53.9 cm^{-1}.

The frequency lines in Fig. 5 show that there is good agreement between our calculated vibrational modes and previous experimental data. They also show that there are significant differences in the THz spectra of all-*trans* and 9-*cis* retinal in frequency shifts as well as in relative intensities. For example, 9-*cis* retinal shows a peak at 24.40 cm^{-1} that was assigned to a bending of the chain out of the plane and all-*trans* retinal does not. Also, all-*trans* retinal has a peak at 48.31 cm^{-1}, which represents a torsion around the first double bond of the chain that is missing in the spectrum of 9-*cis* retinal. Furthermore, the intensities of the different peaks common in both spectra show significant differences.

6. Conclusion

This paper has shown that much research has been carried out on the retinal molecule and its proteins. There is a large amount of infrared data available, but only few studies of the far-infrared region, the THz Gap, are known. Through ab initio modelling we have found THz frequencies for two isomers of retinal: all-*trans* retinal and 9-*cis* retinal. Previous data in this low frequency range (0.1–10 THz) is scarce. Our data fits well with the existing data and has allowed us to carry out a simplified assignment of the vibrational modes. Our results also show that in this frequency range there are significant differences in the spectra of the all-*trans* and 9-*cis* isomers, which suggest proceeding with experimentation at these lower frequencies as well as further modelling of 11-*cis* and 13-*cis* retinal. From frequency versus intensity plots of our data it would be interesting to explore differences between the spectra of these isomers in the 10–40 cm^{-1} range experimentally.

There are a number of open questions, of significance to biologists, for future work that motivate the present work. The retinal chromophore exists in a number of different states and future experiments of interest are to determine if T-rays can distinguish the following states: (i) 11-*cis* retinal (unbound, or loosely bound to a chaperone protein), (ii) rhodopsin, with 11-*cis* retinal covalently bound by a protonated Schiff base (SB), (iii) various short-lived intermediates, with all-*trans* retinal and protonated SB, (iv) metarhodopsin II, with all-*trans* retinal and unprotonated SB, (v) metarhodopsin III, with all-*trans* retinal and a reprotonated SB, (vi) all-*trans* retinal (unbound, or loosely bound to a chaperone protein), (vii) all-*trans* retinol (unbound, or loosely bound to a chaperone protein), (viii) chromophore bound to a phospholipid, and (ix) another complete cycle in the retinal pigment epithelium, which isomerizes the all-*trans* retinal back to the 11-*cis* form. Such studies will use both modelling and experimentation. It is only from a combination of structural, spectral and biochemical studies that a complete picture of the structure and dynamics of biologically important molecules can be determined.

Acknowledgements

The authors would like to thank Trevor D. Lamb, John Curtin School of Medical Research, Australian National University, Canberra, for his useful comments on the manuscript and Magdalene Addicoat, School of Chemistry and Physics, the University of Adelaide, for useful discussions on molecular modelling. Funding from the Australian Research Council (ARC) and the Sir Ross and Sir Keith Smith Fund is gratefully acknowledged.

References

[1] R.R. Nigmatullin, V.A. Toboev, G. Smith, P. Butler, J. Phys. D: Appl. Phys. 36 (8) (2003) 1044–1052.
[2] A.G. Ryder, J. Forensic Sci. 47 (2) (2002) 275–284.
[3] E.T.J. Nibbering, H. Fidder, E. Pines, Ann. Rev. Phys. Chem. 56 (2005) 337–637.
[4] A.H. Zewail, Science 242 (1988) 1645–1653.
[5] S.A. Kovalenko, N. Eilers-Koenig, T.A. Senyushkina, N.P. Ernsting, J. Phys. Chem. A 105 (2001) 4834–4843.
[6] F. Schotte, M.H. Lim, T.A. Jackson, A.V. Smirnov, J. Soman, J.S. Olson, G.N. Phillips, M. Wulff, P.A. Anfinrud, Science 300 (2003) 1944–1947.
[7] A. Plech, M. Wulff, S. Bratos, F. Mirloup, R. Vuilleumier, F. Schotte, P.A. Anfinrud, Phys. Rev. Lett. 92 (2004) 125505.
[8] C.-Y. Ruan, V.A. Lobastov, F. Vigliotti, S.Y. Chen, A.M. Zewail, Science 304 (2004) 180–184.
[9] G. Cerullo, S. De Silvestri, Rev. Sci. Instrum. 74 (2003) 1–18.
[10] R.A. Kaindl, M. Wurm, K. Reimann, P. Hamm, A.M. Weiner, M. Woerner, J. Opt. Soc. Am. B 17 (2000) 2086–2094.
[11] A. Markelz, S. Whitmire, J. Hillebrecht, R. Birge, Phys. Med. Biol. 47 (21) (2002) 3797–3805.
[12] T.J. Rainsford, S.P. Mickan, D. Abbott, Proc. SPIE Smart Struct. Devices Syst. II 5649 (2005) 826–838.
[13] P.F. Taday, I.V. Bradley, D.D. Arnone, M. Pepper, J. Pharm. Sci. 92 (4) (2002) 831–837.
[14] P.F. Taday, Phil. Trans. R. Soc. Lond. A 362 (2004) 351–364.
[15] N.R. Arutyunyan, N.N. Brandt, A.Y. Chikishev, S.I. Lebedenko, O.D. Parashchuk, A.P. Razzhivin, Fluctuat. Noise Lett. 5 (2) (2005) 233–241.
[16] L. Duvillaret, F. Garet, J.L. Coutaz, IEEE J. Sel. Top. Quant. Electron. 2 (3) (1996) 739–746.
[17] G. Gallot, D. Grischkowsky, J. Opt. Soc. Am. B: Opt. Phys. 16 (8) (1999) 1204–1212.
[18] K. Suto, J. Nishizawa, Int. J. Infrared Millimeter Waves 26 (7) (2005) 937–952.

[19] M. Walther, P. Plochocka, B. Fischer, H. Helm, P. Uhd Jepsen, Biopolymers 67 (4/5) (2002) 310–313.
[20] B. Fischer, M. Hoffmann, H. Helm, G. Modjesch, P.U. Jepsen, Semicond. Sci. Technol. 20 (7) (2005) 246–253.
[21] P.C. Upadhya, Y.C. Shen, A.G. Davies, E.H. Linfield, Vib. Spectrosc. 35 (1/2) (2004) 139–143.
[22] G. Tiana, R.A. Broglia, L. Sutto, D. Provasi, Molec. Simul. 31 (11) (2005) 765–771.
[23] R.R. Birge, N.B. Gillespie, E.W. Izaguirre, A. Kusnetzow, A.F. Lawrence, D. Singh, Q.W. Song, E. Schmidt, J.A. Stuart, S. Seetharaman, K.J. Wise, J. Phys. Chem. B 103 (49) (1999) 10746–10766.
[24] Z. Chen, R.R. Birge, Trends Biotechnol. 11 (7) (1993) 292–300.
[25] L. Lensu, M. Frydrych, C. Aschi, J. Parkkinen, S. Parkkinen, T. Jaaskelainen, Int. Conf. Comput. Nanosci. (2001) 17–20.
[26] D. Sampedro, A. Migani, A. Pepi, E. Busi, R. Basosi, L. Latterini, F. Elisei, S. Fusi, F. Ponticelli, V. Zanirato, M. Olivucci, J. Am. Chem. Soc. 126 (30) (2004) 9349–9359.
[27] H. Kandori, Y. Shichida, T. Yoshizawa, Biochemistry (Moscow) 66 (11) (2001) 1197–1209.
[28] T.D. Lamb, E.N. Pugh Jr., Prog. Retin. Eye Res. 23 (2004) 307–380.
[29] R.C. Hardie, P. Raghu, Nature 413 (2001) 186–193.
[30] G. Wolf, Nutr. Rev. 62 (Part 1 7) (2004) 283–286.
[31] V. Kuksa, Y. Imanishi, M. Batten, K. Palczewski, A.R. Moise, Vision Res. 43 (28) (2003) 2959–2981.
[32] M. Walther, B. Fischer, M. Schall, H. Helm, P.U. Jepsen, Chem. Phys. Lett. 332 (2000) 389–395.
[33] F.L. Gervasio, G. Cardini, P.R. Salvi, V. Schettino, J. Phys. Chem. A 102 (1998) 2131–2136.
[34] A. Bifone, H.J.M. deGroot, F. Buda, Chem. Phys. Lett. 248 (3/4) (1996) 165–172.
[35] C. Morari, D. Bogdan, Spectrochim. Acta—Part A: Molec. Biomolec. Spectrosc. 61 (8) (2005) 1881–1886.
[36] S.W. Lin, M. Groesbeek, I. van der Hoef, P. Verdegem, J. Lugtenburg, R.A. Mathies, J. Phys. Chem. B 102 (15) (1998) 2787–2806.
[37] W. Gartner, L. Losi, Trends Microbiol. 11 (9) (2003) 405–407.
[38] J.L. Spudich, C.-S. Yang, K.-H. Jung, E.N. Spudich, Annu. Rev. Cell Dev. Biol. 16 (2000) 365–392.
[39] D. Oesterhelt, Israel J. Chem. 35 (3/4) (1995) 475–494.
[40] J.K. Lanyi, Annu. Rev. Biophys. Biophys. Chem. 15 (1986) 11–28.
[41] S.A. Shukolyukov, J. Evol. Biochem. Physiol. 26 (4) (1990) 429–444.
[42] J.L. Spudich, D.N. Zacks, R.A. Bogomolni, Israel J. Chem. 35 (3/4) (1995) 495–513.
[43] Y. Mukohata, K. Ihara, T. Tamura, Y. Sugiyama, J. Biochem. 125 (4) (1999) 649–657.
[44] J.K. Lanyi, Annu. Rev. Physiol. 66 (2004) 665–688.
[45] T. Hirai, S. Subramaniam, Fed. Eur. Biochem. Soc. Lett. 545 (1) (2003) 2–8.
[46] T.P. Sakmar, R.P. Franke, H.G. Khorana, Proc. Natl. Acad. Sci. 86 (1989) 8309–8313.
[47] K. Nakanishi, Pure Appl. Chem. 63 (1) (1991) 161–170.
[48] I.H.M. van Stokkum, R.H. Lozier, J. Phys. Chem. B 106 (13) (2002) 3477–3485.
[49] Z. Dancshazy, R. Govindjee, T.G. Ebreyg, Biophys. J. 53 (2) (1988) 379.
[50] H.G. Khorana, J. Biol. Chem. 263 (16) (1988) 7439–7442.
[51] J.K. Lanyi, Experientia 49 (6/7) (1993) 514–517.
[52] U. Haupts, Annu. Rev. Biophys. Biomolec. Struc. 28 (1999) 367–399.
[53] R.W. Schoenlein, L.A. Peteanu, R.A. Mathies, C.V. Shank, Science 254 (5030) (1991) 412–415.
[54] M.J. Marinissen, J.S. Gutkind, Trends Pharmacol. Sci. 22 (7) (2001) 368–376.
[55] H. Kandori, H. Sasabe, K. Nakanishi, T. Yoshizawa, T. Mizukami, Y. Shichida, J. Am. Chem. Soc. 118 (1996) 1002–1005.
[56] K. Wynne, R.M. Hochstrasser, Chem. Phys. 171 (1/2) (1993) 179–188.
[57] K. Wynne, G.D. Reid, R.M. Hochstrasser, J. Chem. Phys. 105 (6) (1996) 2287–2297.
[58] R. Henderson, J. Mol. Biol. (1975) 123–138.
[59] R. Henderson, J.M. Baldwin, T.A. Ceska, F. Zemlin, E. Beckmann, K.H. Downing, J. Mol. Biol. 213 (1990) 899–929.
[60] S. Subramaniam, M. Lindahl, P. Bullough, A.R. Faruqi, J. Tittor, D. Oesterhelt, L. Brown, J. Lanyi, R. Henderson, J. Mol. Biol. 287 (1999) 145–161.
[61] E. Pebay-Peyroula, G. Rummel, J.P. Rosenbusch, E.M. Landau, Science 277 (1997) 1676–1681.
[62] H. Luecke, H.T. Richter, J.K. Lanyi, Science 280 (1998) 1934–1937.
[63] S. Subramaniam, T. Hirai, R. Henderson, Philos. Trans. R. Soc. Lond. Ser. A: Math. Phys. Eng. Sci. 360 (1794) (2002) 859–874.
[64] H. Luecke, B. Schobert, H.-T. Richter, J.-P. Cartailler, J.K. Lanyi, Science 286 (1999) 255–260.
[65] T. Okada, M. Sugihara, A.N. Bondar, M. Elstner, P. Entel, V. Buss, J. Mol. Biol. 342 (2) (2004) 571–583.
[66] R. Neutze, E. Pebay-Peyroula, K. Edman, A. Royant, J. Navarro, Landau Em Biochimica et Biophysica Acta-Biomembr. 1565 (2) (2002) 144–167.
[67] J.B. Ames, S.P.A. Fodor, R. Gebhard, J. Raab, E.M.M. van den Berg, J. Lugtenburg, R.A. Mathies, Biochemistry 28 (1989) 3681–3687.
[68] S.P. Fodor, J.B. Ames, R. Gebhard, E.M. van der Berg, W. Stoeckenius, J. Lugtenburg, R.A. Mathies, Biochemistry 27 (1988) 7097–7101.
[69] R.A. Mathies, S.O. Smith, I. Palings, Biol. Appl. Raman Spectrosc. 2 (1987) 59–108.
[70] K.J. Rothschild, O. Bousche, M.S. Braiman, C.A. Hasselbacher, J.L. Spudich, Biochemistry 27 (1988) 2420–2424.
[71] C. Pande, J.K. Lanyi, R.H. Callender, Biophys. J. 55 (1989) 425–431.
[72] S.O. Smith, M.J. Marvin, R.A. Bogomolni, R.A. Mathies, J. Biol. Chem. 259 (1984) 12326–12329.
[73] S.O. Smith, A.B. Myers, J.A. Pardoen, C. Winkel, P.P.J. Mulder, J. Luetenburg, R.A. Mathies, Proc. Natl. Acad. Sci. 81 (1984) 2029–2055.
[74] I.M. Pepe, Prog. Retin. Eye Res. 20 (6) (2001) 733–759.
[75] S.P.A. Fodor, R. Gebhard, J. Lutgenburg, R.A. Bogomolni, R.A. Mathies, J. Biol. Chem. 264 (31) (1989) 18280–18283.
[76] M.L. Applebury, K.S. Peters, P.M. Rentzepis, Biophys. J. 23 (1978) 375–382.
[77] E.P. Ippen, C.V. Shank, A. Lewis, M.A. Marcus, Science 200 (1978) 1279–1281.
[78] A.V. Sharkov, A.V. Pakulev, S.V. Chekalin, Y.A. Matzveetz, Biochim. Biophys. Acta 808 (94) (1985) 94–102.
[79] M.C. Nuss, W. Zinth, W. Kaiser, E. Kolling, D. Oesterhelt, Chem. Phys. Lett. 117 (1) (1985) 1–8.
[80] H.-J. Polland, M.A. Franz, W. Zinth, W. Kaiser, E. Kolling, D. Oesterhelt, Biophys. J. 49 (1986) 651–662.
[81] S.J. Doig, P.J. Reid, R.A. Mathies, J. Phys. Chem. 95 (16) (1991) 6372–6379.
[82] L.A. Peteanu, R.W. Schoenlein, Q. Wang, R.A. Mathies, C.V. Shank, Proc. Natl. Acad. Sci. 90 (1993) 11762–11766.
[83] Q. Wang, R.W. Schoenlein, L.A. Peteanu, R.A. Mathies, C.V. Shank, Science 266 (5184) (1994) 422–424.
[84] G.G. Kochendoerfer, R.A. Mathies, Israel J. Chem. 35 (1995) 211–226.
[85] R.A. Mathies, Novartis Foundation Symposium, John Wiley and Sons, 1999, pp. 70–84.
[86] R.S. Becker, K.J. Freedman, J. Am. Chem. Soc. 107 (1985) 1477–1485.
[87] Y. Koyama, K. Kubo, M. Komori, H. Yasuda, Y. Mukai, Photochem. Photobiol. 54 (1991) 433–443.
[88] H.J.A. Dartnall, Vision Res. 8 (1967) 339–358.
[89] L. Senak, Z.M. Ju, N. Noy, R. Callender, D. Manor, Biospectroscopy 3 (2) (1997) 131–142.
[90] D. Gill, M.E. Heyde, L. Rimai, J. Am. Chem. Soc. 93 (1971) 6288–6289.
[91] L. Rimai, D. Gill, J.L. Parsons, J. Am. Chem. Soc. 93 (1971) 1353–1357.
[92] M.E. Heyde, D. Gill, R.G. Kilponen, L. Rimai, J. Am. Chem. Soc. 93 (1971) 6776–6780.
[93] P.H. Siegel, Int. J. High Speed Electron. Syst. 13 (2) (2003) 351–394.
[94] B. Ferguson, X.-C. Zhang, Nature Mater. 1 (26) (2002) 26–33.
[95] X.-C. Zhang, Phil. Trans. R. Soc. Lond. A 362 (2004) 283–299.
[96] M.J. Fitch, R. Osiander, Johns Hopkins Appl. Tech. Digest 25 (4) (2004) 348–355.
[97] D.L. Woolard, E.R. Brown, M. Pepper, M. Kemp, Proc. IEEE 93 (10) (2005) 1722–1743.

[98] S. Wang, B. Ferguson, D. Abbott, X.-C. Zhang, J. Biol. Phys. 29 (2003) 247–256.
[99] B. Ferguson, S. Wang, D. Gray, D. Abbott, X.-C. Zhang, Opt. Lett. 27 (15) (2002) 1312–1314.
[100] B. Ferguson, S. Wang, D. Gray, D. Abbott, X.-C. Zhang, Microelectron. J. 33 (12) (2002) 1043–1051.
[101] X.-C. Zhang, Phys. Med. Biol. 47 (21) (2002) 3667–3677.
[102] A. Quema, H. Takahashi, M. Sakai, M. Goto, S. Ono, N. Sarukura, R. Shioda, N. Yamada, Jpn. J. Appl. Phys. Part 2-Lett. 42 (8A) (2003) L932–L934.
[103] S. Nishizawa, K. Sakai, T. Hangyo, T. Nagashima, M.W. Takeda, K. Tominaga, A. Oka, K. Tanaka, O. Morikawa, Terahertz Optoelectron. Top. Appl. Phys. 97 (2005) 203–269.
[104] S.P. Mickan, A. Menikh, H. Liu, C.A. Mannella, R. MacColl, D. Abbott, J. Munch, X.-C. Zhang, Phys. Med. Biol. (IOP) 47 (2002) 3789–3795.
[105] S.W. Smye, J.M. Chamberlain, A.J. Fitzgerald, E. Berry, Phys. Med. Biol. 46 (2001) 101–112.
[106] M.K. Choi, A. Bettermann, D.W. van der Weide, Philos. Trans. R. Soc. Lond. Ser. A: Math. Phys. Eng. Sci. 362 (1815) (2004) 337–347.
[107] R.M. Woodward, V.P. Wallace, D.D. Arnone, E.H. Linfield, M. Pepper, J. Biol. Phys. 29 (2/3) (2003) 257–261.
[108] N. Nagai, R. Kumazawa, R. Fukasawa, Chem. Phys. Lett. 413 (4–6) (2005) 495–500.
[109] W. Shi, Y.J. Ding, Laser Phys. Lett. 1 (11) (2004) 560–564.
[110] M.F. Guest, I.J. Bush, H.J.J. van Dam, P. Sherwood, J.M.H. Thomas, J.H. van Lenthe, R.W.A. Havenith, J. Kendrick, Molec. Phys. 103 (6–8) (2005) 719–747.
[111] M.J. Frisch, et al., Gaussian 94, Revision D.3, Gaussian Inc., Pittsburgh, PA, 1995.
[112] J.A. Wass, Science 290 (5499) (2000) 2098.
[113] G. Schaftenaar, J.H. Noordik, J. Comput.-Aided Mol. Design 14 (2000) 123–134.
[114] F. Blomgren, S. Larsson, J. Comp. Chem. 26 (7) (2005) 738–742.
[115] U.F. Rohrig, L. Guidoni, A. Laio, J. Am. Chem. Soc. 126 (47) (2004) 15328–15329.